EXPERIMENTAL AND NUMERICAL INVESTIGATIONS ON THE OPERATION OF THE HYPERSONIC LUDWIEG TUBE BRAUNSCHWEIG

Malte Estorf, Torsten Wolf, and Rolf Radespiel

Technical University at Braunschweig, Institute for Fluid Mechanics, Bienroder Weg 3, 38106 Braunschweig, Germany, Email: m.estorf@tu-braunschweig.de

ABSTRACT

In summer 2003 the Hypersonic Ludwieg Tube Braunschweig (HLB) has been commissioned. It has been designed for Machnumber M = 6. The operative range of the unit Reynoldsnumber is between $3 \cdot 10^6\ {}^1\!/\mathrm{m}$ and $20 \cdot 10^6\ {}^1\!/\mathrm{m}$. The test section has 500 mm diameter and the run time with near steady flow conditions is 80 ms. First measurements of the pitot pressure within the testsection have shown good transverse uniformity, but measurements of the total temperature within the storage tube revealed a strong stratification accompanied by convective flow within the heated section of the tube. In this paper we present recent measures to attenuate the stratification. Measurements of the temperature distribution within the testsection and preliminary transition tests on a sharp 5° half-angle cone have been performed. Further we compare first results of invisvid numerical simulations of the unsteady onset of flow in the HLB to measured data.

Key words: hypersonic flow, Ludwieg tube, flow measurement techniques, transition, numerical flow simulation.

1. NOMENCLATURE

a	:	speed of sound
A	:	crossectional area
M	:	Mach number
l	:	characteristic Length
L	:	tube length
p	:	pressure
Re	:	Reynolds number
St	:	Stanton number
t_m	:	measurement time
T	:	temperature
u	:	velocity
X, Z	:	coordinates in the test section
κ	:	ratio of specific heats

Subscripts

h	:	concerning the heated section of the tube
c	:	concerning the cold section of the tube
pit	:	quantity behind a normal shock
t	:	total quantity
vac	:	initial quantity in vacuum section
0	:	in front of expansion wave in the tube
1	:	behind expansion wave in the tube
2	:	after expansion in the nozzle
$*$	:	in the nozzle throat

2. INTRODUCTION

Aerothermal design of reusable reentry vehicles requires good knowledge of thermal loads on all structural components. Although numerical methods for hypersonic flow simulation are already well developed the experimental proof is still essential. Because of their low operational cost and good flow quality Ludwieg tube type cold blowdown tunnels are of special interest. They need no total pressure control device or large settling chamber as conventional blow-down facilities do. The operational effort for Ludwieg type tunnels can be further reduced by the use of a fast acting valve instead of the bursting diaphragm originally suggested by Ludwieg (Ludwieg 1955). The development of a Ludwieg tube with such a valve in the throat of the hypersonic nozzle is documented in (Koppenwallner et al. 1993). According to the facility described there a new hypersonic wind tunnel has been built and commissioned at the Institute of Fluid Mechanics in Braunschweig over the last year. During the design of the hypersonic nozzle extensive Navier-Stokes calculations have been conducted in order to optimize the contour of the nozzle throat and the straightening section considering the displacement thickness of turbulent nozzle wall boundary layers. With an optimized nozzle contour the nonuniformity in pitot pressure within the test section due to the wake of the valve turned out to have the same magnitude as the remaining nonuniformities due to the expansion and compression waves from the nozzle (Kožulović et al. 2002). First measurenments of the pitot pressure in the test section have been presented in (Estorf et al. 2003). They showed a deviation of about $\pm 1.2\%$ over a vertical transverse through the test section. But those measurements suffered from a disfunction of the storage tube heating and could not be conducted with the windtunnel running at its design temperature. Most of the measurements where conducted without any heating and therefore with too low ratio of flow total temperature to nozzle wall temperature and with the uncertainty of possible condensation effects in the test section.

We can now report on an improved operation of the heating and update the measured pitot pressures. We also present measurements of the flow recovery temperature in the test section. Further the results of preliminary transition tests on a sharp 5° half-angle cone are shown. The aim of the latter was to qualitatively assess the relative acoustic disturbance environment of the HLB by comparing the smooth wall transition onset locations to those of other Mach 6 tunnels. Results of numerical simulations of the time-dependent flow field in the HLB are presented in order to examine the complex flow phenomena

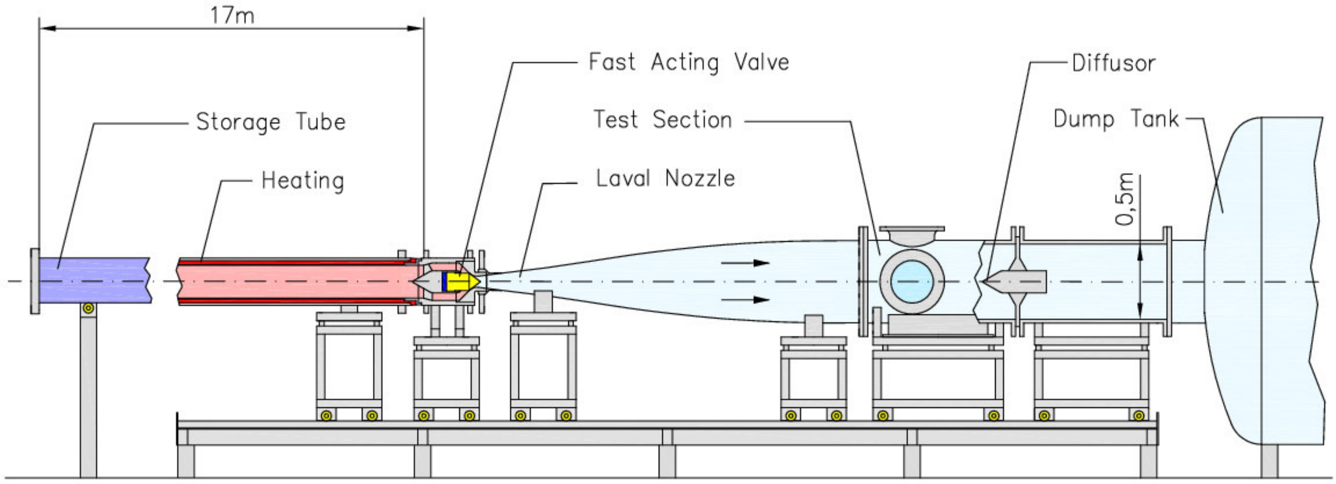

Figure 1. Sketch of the HLB

during the onset of the flow. The effects of these transient phenomena on the flow around wind tunnel models in the test section must be quantitatively determined in order to qualify the tunnel for accurate heat transfer measurements. Results are shown for the total runtime of the tunnel on a simplified geometry with a membrane instead of a valve. Preliminary results for the actual geometry including the valve opening are also presented. The paper is divided into three sections. First we give an extensive description of the new test facility and provide some basic equations describing the thermodynamic characteristics which are considered later on. Second the experimental and numerical methods are outlined including the description of the measurement technique and data reduction. Third we present and discuss the results.

3. FACILITY DESCRIPTION

3.1 Working Principle

A schematic diagram of the HLB is given in Fig. 1. The assembly is devided into a high pressure and a low pressure section, which are seperated by the fast acting valve. The high pressure section consisting of the 17 m long storage tube with a 3 m long heated section can be pressurized to up to 30 bar. The low pressure section consisting of the hypersonic nozzle, the test section, the diffusor and a 6 m^3 dump tank is evacuated before each run to about 1 mbar. The valve basically consists of a pneumatically driven piston which fits into the nozzle throat with its conical end. The valve can be opened for about 100 ms. This causes an expansion wave to run into the storage tube. In the wave the air is accelerated towards the nozzle where it is further expanded and accelerated to Mach 5.9 in the testsection. The expansion wave traveling through the storage tube is reflected at its end and reaches the valve again after about 90 ms. This is the time period of steady flow conditions in the test section. The closure of the valve inhibits complete equalisation of pressure in the facility, which saves energy and time. The total energy cost for one run is remarkably low. It can be estimated to be less than 1 EUR. The cycle time for subsequent runs is about 6 minutes.

3.2 Design Details

The expansion of the gas in the nozzle reduces its static temperature by a factor of 8. That causes the gas to fall below its saturation curve if it is not heated previously. It is sufficient to heat only that part of the storage tube that contains the air which is pushed out during one run. The partially heated tube implies a step in the tube temperature which has to be compensated by a step in the tube diameter in order to avoid disturbances from the step to be reflected upstream when the expansion wave passes. Fig. 2 shows the process in the x, t-plane. The expansion wave starting from the nozzle ($x = 0$) propagates with the speed of sound into the tube which is a_{0h} in the heated and a_{0c} in the cold section. It passes the step without reflection if the pressure ratio across the expansion does not

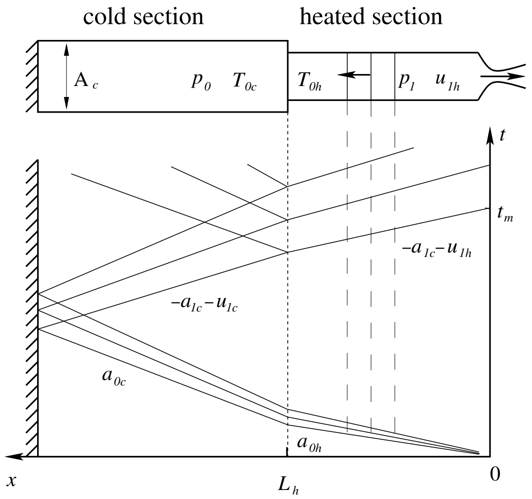

Figure 2. Diagram of expansion wave in the x,t-Plane

change at the step. The latter is (Becker 1966)

$$\frac{p_1}{p_0} = \left(1 + \frac{\kappa - 1}{2} M_1\right)^{\frac{-2\kappa}{\kappa-1}} \tag{1}$$

The Mach number M_1 is only a function of the ratio between the velocity behind the expansion and the speed of its propagation $\frac{u_1}{a_0}$. Using $a_o \propto \sqrt{T_0}$ and $u_{1c}A_c = u_{1h}A_h$ [1] the necessary relation between the change of temperature and area for no reflection is

$$A_h \cdot \sqrt{T_h} = A_c \cdot \sqrt{T_c}\ . \tag{2}$$

This relation is fulfilled in the HLB at the design temperature of 650 K in the heated section which has a diameter of 210 mm.

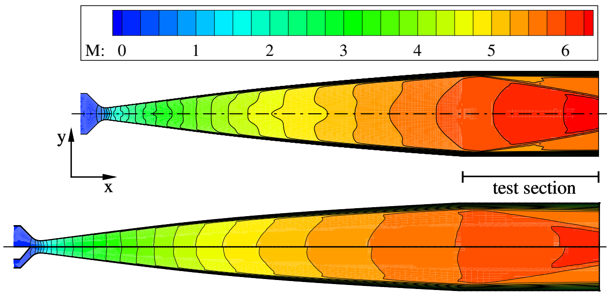

Figure 3. Calculated Mach number distribution in a nozzle with preliminary design (upper) and in the final design nozzle (lower). The latter with and without valve body in the lower and upper nozzle half respectively.

The diameter of the nozzle throat is 70 mm and the nozzle expands to 496 mm in the test section. The diverging part of the nozzle is carefully contoured in order to have only a small Mach number gradient in the test section. Its opening half angle varies from initially $7.5°$ to $3°$ at the nozzle end that is some flow expansion is maintained into the test section in order to have the nozzle flow insensitive to deviations of the design point. During the design of the nozzle Navier-Stokes calculations have been conducted in order to account for the contribution of boundary layer displacenment thickness to the effective nozzle contour which should not be neglected in long hypersonic nozzles. The nozzle contour was chosen as picewise analytical functions which allowed to control the contour curvature (for details see (Kožulović et al. 2002)). Fig. 3 shows calculated Mach number contours in a nozzle with preliminary design at the top and in the final design nozzle at the bottom. The uniformity of Mach number distribution in the test section could be improved by careful variation of the nozzle geometry especially in the throat region. At the same time the influence of the valve body seated in front of the nozzle on the axis of the tube was studied. The bottom diagram of Fig. 3 shows the results of calculations with and without the valve body in the lower and upper nozzle half. The wake of the valve can be seen in the Mach number countours but its influence on nonuniformity is about the same as the remaining nonuniformity in the optimized nozzle without the valve.

[1] This is approximatly true for the low mach number of $M = 0.05$ in the HLB tube.

4. EXPERIMENTAL METHOD

4.1 Pressure Measurements

A Pitot rake is used to calibrate the flow in the test section as displayed in Fig. 4. The rake is electrically traversed in $X-$ and $Z-$ directions on tracks mounted in a housing below the test section. The pressure sensors are located within the rake just behind the Pitot tubes. We use sensors of SCC15A type by Sensortechniques. These sensors measure the absolute pressure against an internal vacuum by means of a piezo resistance crystal. The Wheatstone measuring bridge receives its power supply from a battery. Data acquisition is performed using a multifunctional PC card of National Instruments. The sampling rate is at 2.5 kHz which matches the given temporal resolution of the pressure sensor. The temporal distribution of the driver tube pressure is measured in the valve section, in between the valve mounting struts. This pressure sensor is connected to the measurement orifice via a short flexible tube in order to isolate it from the mechanical oscillations that occur during the runs. Using the pressure drop at this position one can determine the Mach number M_1 in the driver tube according to Equation 1. This allows to determine the total pressure, p_{1t}, in the driver tube from

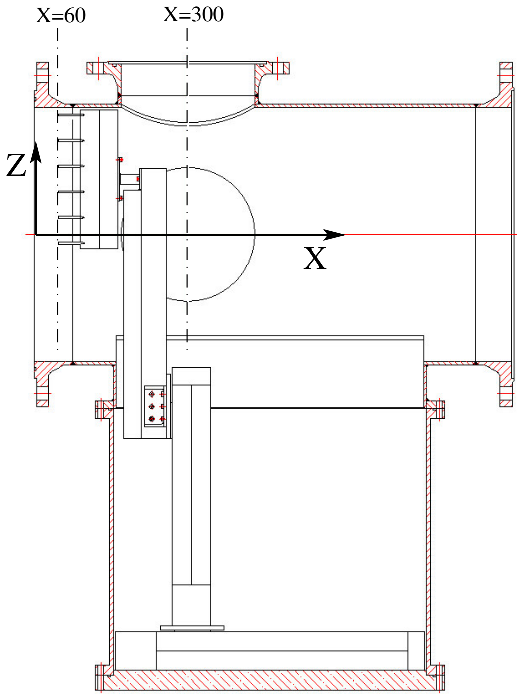

Figure 4. Diagram of the measurement section with Pitot rake and XZ-Traverse

$$\frac{p_1}{p_{1t}} = \left(1 + \frac{\kappa - 1}{2} {Ma_1}^2\right)^{\frac{\kappa}{1-\kappa}} \tag{3}$$

The total pressure of the flow into the nozzle, p_{1t}, is needed to determine the local Mach number in the test section from the well-known Rayleigh-Pitot-formula once the Pitot pressure has been measured there. A mercury filled, inclined U-tube served as a pressure gauge for calibration of the Pitot pressure sensors. One of the legs was evacuated to a constant pressure of 10^{-2} mbar. The other leg was connected to the test section which enabled an in situ calibration. The inclined U-tube allowed to determine the calibration pressures with an accuracy of 0.4 mbar. The test section pressure was thereby varied and the readings of the Wheatstone bridge were connected to the true pressure by linear regression analysis. Repeated measurements revealed that the slope of the regression line was reproduced very well but the zero-pressure voltage varied considerably. This posed no problem in practical operations as the zero-pressure voltage can be measured easily before every tunnel run. For constant temperatures in the laboratory one could then determine the total measurement error as ± 0.7 mbar. Note that a significant sensitivity of the measured pressures with respect to the temperature was detected. This error is caused by changes of the temperature in the laboratory hall rather than by aerodynamic heating of the rake structure during the individual tunnel runs.

4.2 Temperature Measurements

The temperature was measured in the storage tube and in the test section with Nickel-Chrome/Nickel thermocouples. The diameter of the thermocouple wires was 0.04 mm. They where soldered up to a 0.2 mm spheric junction. The thermoelectric voltage was low-pass filtered at 500 Hz and recorded by a commercial measurement amplifier with internal cold-junction compensation. By measuring temperatures in calm air with five different probes at the same time and position the accuracy of thermocouple wire temperature determination is estimated to be within 0.2 K.

Three probes where placed around the central valve body to measure the nozzle entry temperature of the flow. They were located at the same axial position with an angular offset of 120° starting at the top. The thermocouple wires were conducted into the flow by small diameter tubes with an open ended probe head. Since the flow velocity within the driver tube is very small the recovery temperature at the probe surface does not differ from the total temperature by more then 0.01%. The probe temperature in stationary measurements depends on the ratio of surface heat flux to the thermocouple junction and heat conducted away from the junction into the wire. This ratio is a function of the Biot number built with the wire length and the ratio of fluid contact area to wire cross-sectional area. Both are large enough to neglect the influence of conductive cooling through the wire and to assume the measured temperature is the fluid recovery temperature in stationary conditions. Instantanious temperature measurement accuracy suffers from the response time of the probe which again is a function of Biot number built with the junction diameter. It has to be sufficiently small for fast responding probes which is limited by its mechanical strength. However, the probes with 0.04 mm wire diameter where sufficiently thick to resist the fluid forces in the driver tube. The time required for the junction to reach 63.2 percent of the fluid temperature after a step temperature change is specified by the manufacturer with 4 ms in 17 m/s air flow at atmospheric pressure. Assuming that the heat transfer scales with the square roots of fluid velocity and density which is true for a flat plate with laminar boundary layer, the thermal response time of the probes in the pressurized driver tube can be estimated to be 1 ms. For the temperature measurements in

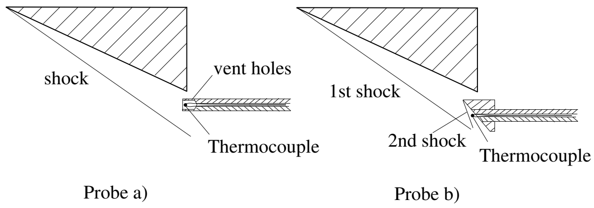

Figure 5. Thermocouple probes used for temperature measurement in the test section

the test section a temperature rake with five thermocouples has been used. Because of the high flow velocities in the test section the probe design has to be a compromise of high recovery factor and fast response time. In common probe design for high speed flow the thermocouple junction is positioned in relatively low speed flow inside a vented chamber formed by the support tube (see refs. (Scadron et al. 1950) and (Albertson & Bausermann Jr. 1993)). First tests with such probe design with different vent to inlet area ratios showed a too long response time compared to the runtime of the HLB. This is due to the low density flow behind the normal shock forming in front of the probe. Therefore two probe designs with one and two oblique shocks in front of the thermocouple junction have been considered. The probes are sketched in Fig. 5 a) and b). Probe b) had the junction directly exposed to the flow without a stagnation chamber. The highest ratio of Reynolds number over a single oblique shock is achieved with a shock angle of 37° corresponding to a body angle of 27° at Mach 5.9. For two subsequent shocks slightly smaller wedge angles have to be used for maximum rise of Reynold number. Both body angles of the used probes where 25° resulting in a calculated Reynolds number ratio of 3.4 over one shock and 6.8 over both shocks.

4.3 Heat Transfer Measurements

A high speed infrared camera was used for temperature measurements on the surface of a 5° half angle cone. The camera was mounted upon the top window of the measurement section which was equipped with a sapphire glass insert. Due to the small diameter of the insert the field of view in the measurement section was restricted to 120 mm. Therefore the heat transfer measurements wihtin the area of interest on the 500 mm long cone could only be performed in subsequent tunnel runs. The spatial calibration of the thermographic images was done by taking an image of a ruler in each camera position. The framerate of the camera was 150 Hz yielding 13 to 14 images per run. Before the measurements a nonuniformity correction matrix for the pixels of the infrared CCD-chip was calculated by taking images of two black plates with different uniform temperature. Correction values for each pixel were calculated accounting for the deviation in offset and slope with respect to the mean of all pixels. The absolute sensitivity was then determined using a black radiator which is basically a cavity in a constant temperature body. The calibration curve was generated by putting the black radiator into the measurement section and varying its temperature over the range expected in the measurements. Camera chip intensity values where read out in steps of one degree Celsius and averaged over a field of 9×9 pixel in the center of the cavities image. Intensities and temperatures were mapped by a third order polynomial fit.

The surface heat flux was calculated from the transient temperature data using a modified Cook and Felderman method (Cook & Felderman 1966) which was regularized by an iterative method (Estorf & Radespiel) in order to reduce the sensitivity to measurement noise due to the standard method's inherent instability. For further noise reduction the temperature values measured on the cone surface have been averaged in rows of 20 pixel length over the span of the cone assuming that the physical temperature does only vary in the axial direction. That is true for exact alignment of the cone axis with the flow direction. Accordingly the alignment of the cone with the flow has been done iteratively in several tunnel runs by changing the inclination carefully in steps of $0.05°$ until the contour lines of equal temperature were symmetric. This was done subsequently with the camera mounted on the top window and at one of the side windows to align the yaw and pitch angles, respectively.

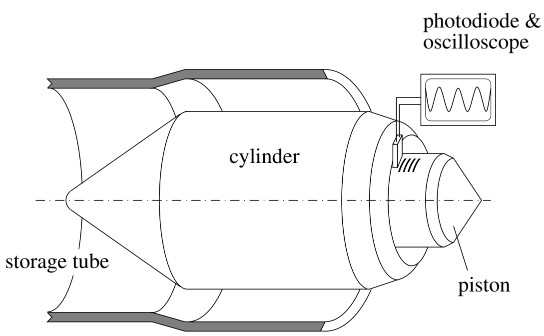

Figure 6. Schematic measurement setup for valve opening

4.4 Valve Opening Measurements

The simulation of the flow field in the HLB requires knowledge about the opening of the valve, i.e. the mean speed of the valve piston as well as the length of the travel. A photodiode was attached to the front of the valve piston while a foil with a pattern of alternating black and white lines was put on the side of the piston (cf. Fig. 6). The width of the lines was 1 mm. Cords were lead out pressure-tight. The alternating voltage signal of the photoelectric relay during opening and closure was recorded and stored by an oscilloscope. The measurement was triggered by the valve-control. The resulting variation of voltage in time shows a mean speed of the piston of 5 m/s. The traverse path is 48.5 mm which is in agreement with the manufacture drawings.

4.5 Model

For transition tests a 500 mm long five degree half angle cone was manufactured. It was made from black perspex (PMMA) with an apex from aluminium. The use of perspex provides low thermometric conductiviy and good emissivity which is needed for thermographic measurement. The surface of the perspex was polished. Unfortunately the quality of the polishment on the first five millimeters from the apex was poor due to the manufacturing technique. The surface roughness there was about 5 µm. The nose diameter of the cone was about 0.24 mm which is two orders of magnitude away from the average molecular free lenth of path. Therefore the nose produces a bow shock implying a thin entropy-layer which might have influence on transition. About 15 mm from the apex at the fit between aluminium and perspex a small circular groove of 0.07 mm depth and 0.26 mm length remained.

5. RESULTS AND DISCUSSION

5.1 Measurements of Test Conditions

Fig. 7 shows the pressure measured during one run at the valve section 200 mm upstream from the nozzle throat. The initial pressure was set to 15 bar for this run and the

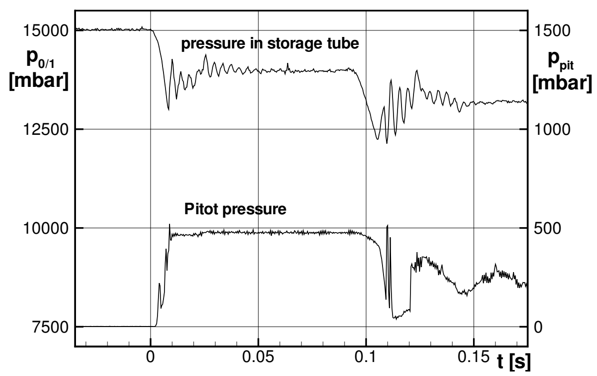

Figure 7. Example for a pressure record in the storage tube and the test section during a run at $p_0 = 15\,\mathrm{bar}$

temperature in the heated section of the storage tube was about 460 K. With the opening of the valve the pressure starts to drop and after some oscillation it reaches a constant value until it drops again after 90 ms which is the time the expansion wave needs to travel back and forth in the tube. The pitot pressure measured at the same time in the center of the test section is remarkably constant throughout the run. After about 110 ms the valve closes which can be seen in the sudden drop of the Pitot pressure after that time. The temperature measured in the valve section is shown in Fig. 8 for a run without heating of the tube. The development of the temperature correlates well with the recording of the pressure. The steep temperature drop after the opening of the valve shows the capability of the thermocouples to follow fast temperature changes in the high density flow in the tube. The upper and lower thermocouples show slightly different temperature values wich is caused by stratification within tube due to previous operation of the heating. When the tube is heated the stratification becomes stronger and due to the large diameter of the tube the temperature differences can become as big as 100 K over the height. Since the storage tube is divided into a heated and a non heated section, which is not isolated, the stratification drives a strong convection along the tube if no counter measures are taken. Fig. 9 shows the temperature recorded during a run with operation of the heating at an early development stage. Since

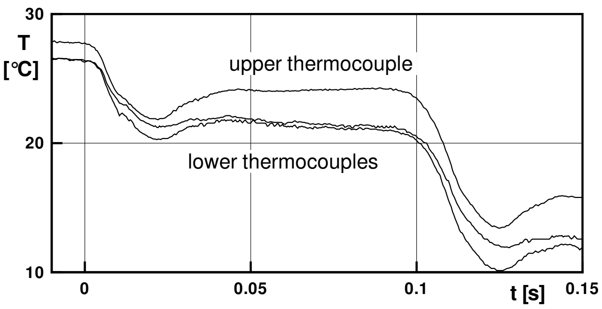

Figure 8. Variation of temperature in front of the nozzle throat during a run without heating

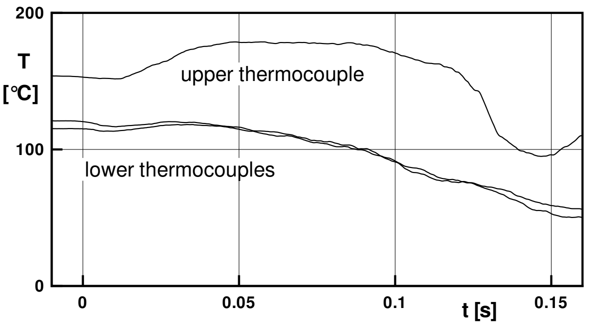

Figure 9. Variation of temperature in front of the nozzle throat during a run with heating (preliminary configuration)

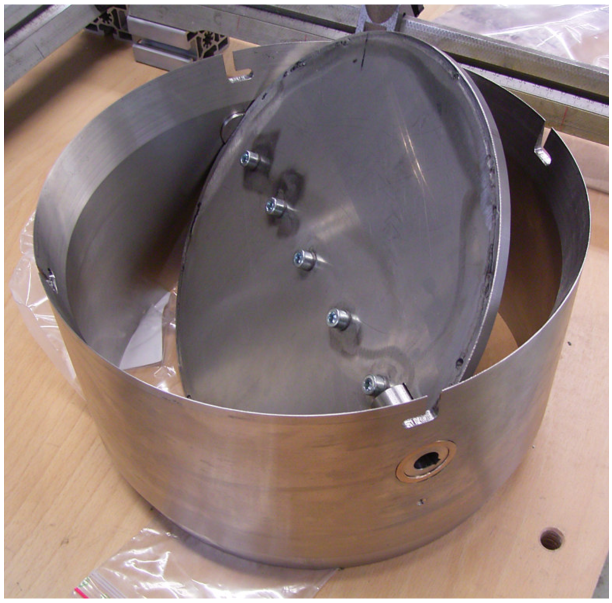

Figure 10. Shutter for heated tube section

the thermocouple measures the temperature at a fixed position, the temporal measurement can be interpreted as a spatial temperature distribution in the air column passing the probe. The measured temperature difference over the heigth of the tube increases in the air arriving from the end of the heated section. A step in the tube temperature which is needed to make up for the step in tube diameter (see section 3.1) cannot be obseved. Moreover the flow of hot air into the upper half of the unisolated tube section imposes thermal stresses to the tube which lift it up from some of its supports. To stop the convection an isolated shutter according to Fig. 10 has recently been installed at the end of the heated section. It is opend only shortly before a run. The crosssectional area blocked by the opened shutter is smaller than the area difference between heated and non heated section. Therefore the shutter should not impose any additional disturbances on the passing expansion wave. The temperatures measured in the tube with operation of the shutter are plotted in Fig. 11. The stratification is reduced to 25 °C at the beginning and 20 °C at the end of the run. The sudden drop of temperature when the air from the end of the heated section passes the probes can now be observed. Since the remaining temperature stratification imposes some uncertainty to the test conditions in the measurement section the temperature there has been measured as well. Two characteristic temperature recordings from probe types a) and b) are shown in Fig. 11. Both were recorded in the same vertical position of the test section, but not in the same run. However, it can be seen that probe b) has a steeper slope at the beginning of the run but converges to smaller value in the end. None of the probes reaches the temperature shown by the probes in the storage tube. This must be due to a low recovery temperature of both probe types. The higher flow velocity which can be expected at probe b) brings about a lower recovery temperature than

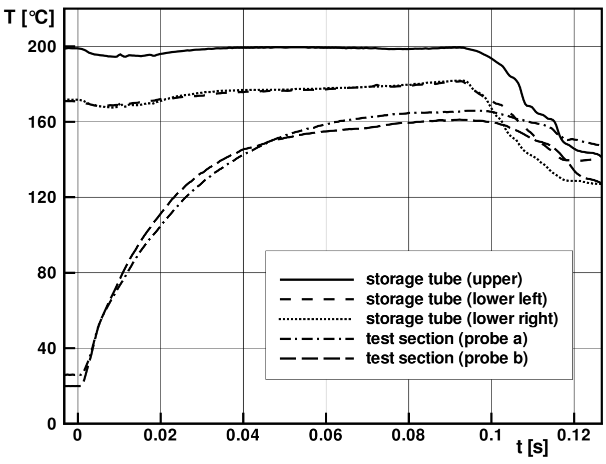

Figure 11. Improved variation of temperature using the shutter; example for time response of probes in the test section

probe a). However, the higher velocity in combination with a higher density flow due to the second shock results in smaller response time. This is promising for future probe design wich should use several shocks and a settling chamber in order to measure more reliable values of the total temperature. For now we show the results of measurements across the test section with the probes we have in Fig. 12. Repeated measurements in some points show deviations of up to 10 °C which is believed to be caused by non reproducable deformations of the thermocouple wire with each run. Deforming the wire manually between the runs resulted in even bigger deviations. At least a trend in the temperatures across the test section can bee seen from the measurements. They show the expected gradient of about 20 °C over the measured height. This results in a 6.5% Reynolds number deviation at the chosen mean storage tube temperature of 460 K.

The Pitot pressures were measured in the test section with and without operation of the heating. Measurements where conducted in the center section from top to bottom at $X = 60\,\mathrm{mm}$ and $X = 300\,\mathrm{mm}$ (see Fig. 4). The results are shown in Figs. 13 and 14 respectively. The initial storage tube pressure was set to 15 bar for the measurement with heating and 7.4 bar for the cold measurement. This was to fit the Reynolds number of a RANS-calculation that had been done previously in the context of valve design. The temperature for the measurements with heating was set to the same value as for the temperature measurements described previously. This results in a mean storage tube temperature of 460 K as can be seen from Fig. 11. The total temperature in the calculation was 600 K. The Pitot pressures measured without heating fit quite well in the center but fall beyond the calculated pressures outside the center. However, the calculated expansion of the flow along the test section which causes the decrease of Pitot pressueres with X is also in good agreement with the measurements. The measurements with heating fit the calculated results very well.

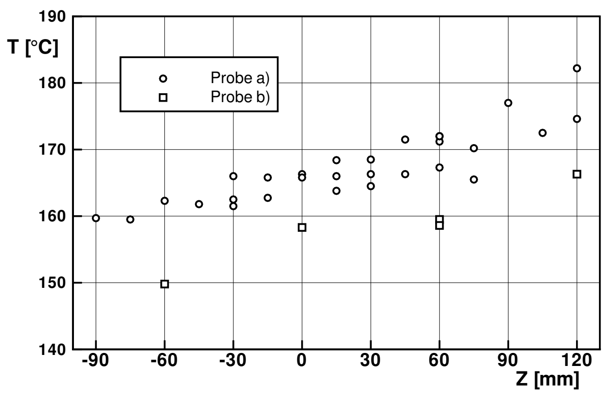

Figure 12. Temperature measured in a vertical traverse in the test section

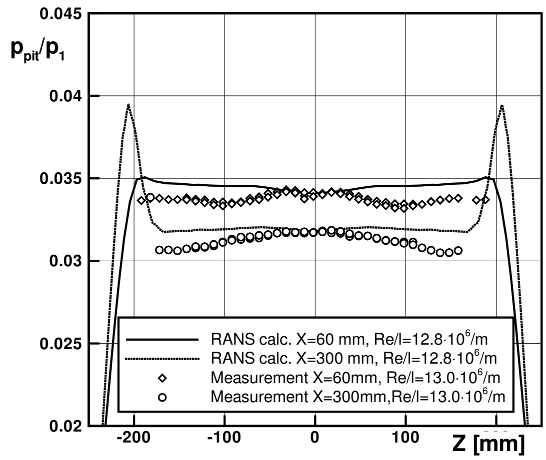

Figure 13. Pitot pressures measured without heating compared to RANS calculation

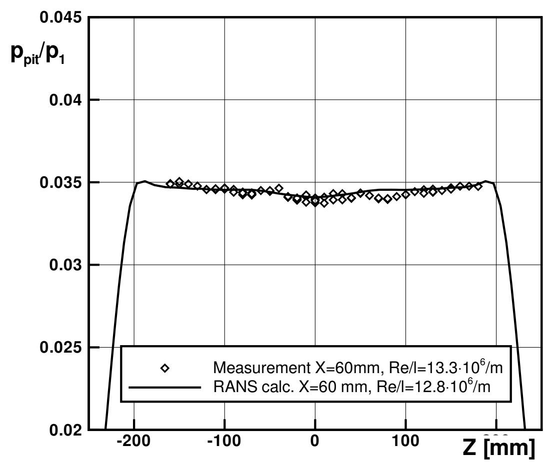

Figure 14. Pitot pressures measured with heating compared to RANS calculation

Not only the pressure level but also the profile showing the wake of the valve body is reproduced by the calculation. Unfortunately for the time being we have no measurement of the pressures with heating in the center section at $X = 300\,\mathrm{mm}$. It will have to be compared to the calculated values in future. The measured pressure deviation over the hight is less than $\pm 1.2\%$. The Mach number was calculated from the Rayleigh-Pitot-formula for both sections. It is $\mathrm{M} = 5.80$ at $X = 60\,\mathrm{mm}$ and between $\mathrm{M} = 5.9$ and $\mathrm{M} = 5.94$ at $X = 300\,\mathrm{mm}$.[2]

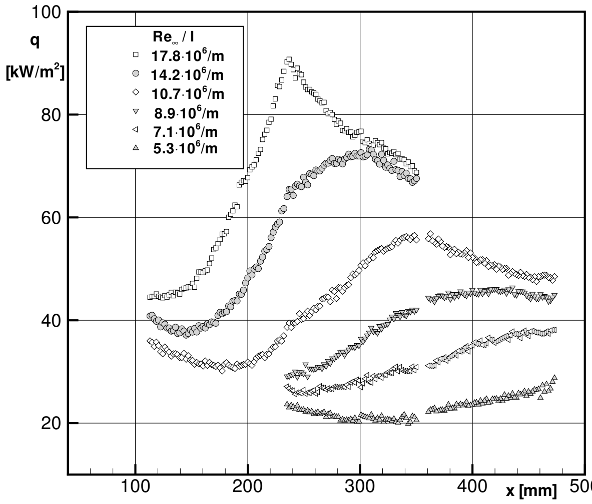

Figure 15. Measured heat flux showing transition on a 5° half angle cone

5.2 Transition Measurements

The transition measurements were conducted with a mean temperature of 460 K in the storage tube. The unit Reynolds number was varied between $Re/l = 5.3 \cdot 10^6\ 1/\mathrm{m}$ and $Re/l = 17.8 \cdot 10^6\ 1/\mathrm{m}$ by varying the initial pressure in the storage tube from $p_0 = 6\,\mathrm{bar}$ to $p_0 = 20\,\mathrm{bar}$. The heat flux values calculated from the temperature data are shown in Fig. 15. The surface temperature rise during one run was only 0.7 K for the low Reynolds number experiments. Since this is only one order of magnitude beyond the noise level of the camera the absolute heat flux values are subject to uncertainty. However, the rise of heat flux due to transition can be seen in all measurements. In Fig. 16 the data is plotted dimensionless with Stanton number versus local Reynolds number. For all unit Reynolds numbers the transition starts at about $Re_x = 2 \cdot 10^6$ with the tendency to move aft with rising unit Reynolds number. This tendency is observed in most conventional hypersonic facilities and is in relationship with tunnel noise (see (Schneider 2001) for a comprehensive list of references). However, compared to other facilities the transition Reynolds numbers measured in the HLB appear to be somewhat lower which might be due to the imperfection of the model we used

[2]We have used $\mathrm{M} = 5.90$ for the calculations of all Reynolds numbers given in this article.

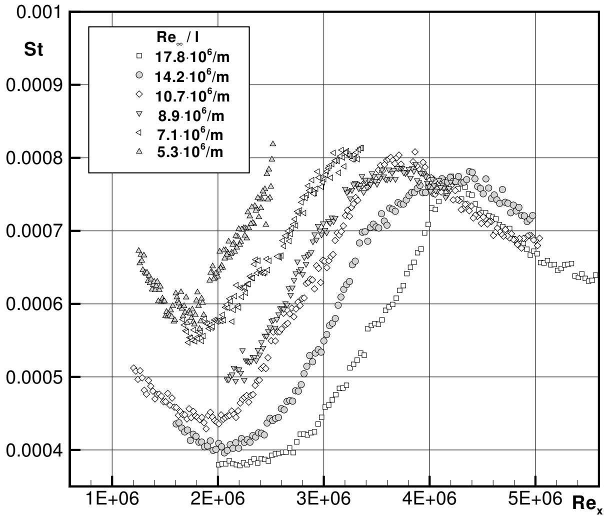

Figure 16. Non-dimensional plot of the measured heat flux data

(see Section 4.5). The effects of bluntness and roughness on hypersonic cone transition are known for some well documented cases which have recently been reviewed in (Schneider 2004). But their discussion with respect to our case of combined deficiencies in model manufacturing would be vague. The experiments will have to be repeated with an enhanced model.

6. NUMERICAL SIMULATIONS

Numerical simulations of the time-dependent flow field in the HLB were performed to examine the complex flow phenomena during the onset of the flow, using the DLR TAU-Code. The TAU-Code (DLR 2004) discretises the Reynolds-averaged Navier-Stokes equations by a finite-volume technique on hybrid grids and has been validated for hypersonic flows in (Mack & Hannemann 2002). Acceleration techniques such as multigrid and residual smoothing are available. For unsteady simulations a dual timestepping approach with an LU-SGS algorithm for the inner iterations was chosen. Fluxes were calculated second-order accurate by the AUSMPW+ upwind scheme. An ideal gas was assumed. The simulations presented are restricted to inviscid flow while future investigations will account for viscous effects.

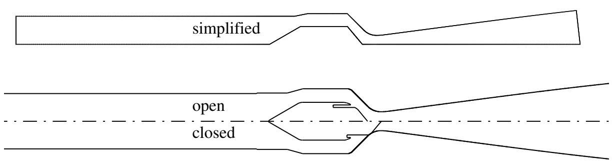

Figure 17. Different HLB contours

To get a first impression of the flow field and to adjust the solver settings a simplified HLB geometry was examined (see Fig. 17). The computational mesh is 2D axisymmetric, has 96330 points and consists of hexaeders only. Instead of a moving valve the contour corresponds to the opened state, while high-pressure and vacuum regimes are separated by a virtual membrane which vanishes at the start of the simulation. The flow conditions are the following: $T_0 = 600\,\mathrm{K}$, $p_0 = 10\,\mathrm{bar}$, $T_{vac} = 295\,\mathrm{K}$ and $p_{vac} = 1\,\mathrm{mbar}$ with the velocity equal to zero throughout the entire domain. The size of the physical timestep was chosen to $\Delta t = 5 \cdot 10^{-8}\,\mathrm{s}$. After the flow is initialised in the fashion of the well-known Riemann problem of gas dynamics, reflections and interaction of expansion and compression waves develop at the contour of the wind tunnel and thus prevent a smooth onset of the flow. The driver tube pressure sensors is located in the valve section 200 mm upstream of the nozzle throat. To compare the results of the simulation with experiments the variation of pressure in time at that location was recorded. Fig. 18 shows the numerical result compared to the measured pressure record taken from Fig. 7. The low-frequency oscillations visible in the experiments partially appear in the simulation. The frequencies are of the same order of magnitude but the oscillations are damped much faster in the simulation. High-frequency oscillations only show up in the simulation and are out of range of the measurement setup in the experimental environment and thus cannot be captured. Reasons for the differences in the low-frequency oscillations may be the simplificaion of the valve modelling, deviations in the temperature distribution in the wind tunnel and of course the negligence of viscous effects in the simulation.

Additional simulations were performed, based on the actual geometry of the wind tunnel including the moving valve piston. In contrast to the simplified geometry, the new computational domain comprises the complete nozzle, the test section and the storage tube to the extent that gas is pushed out during a test run. Except in the vicinity of the piston, the grid is unstructured and becomes coarse towards the end of the storage tube. Therefore the

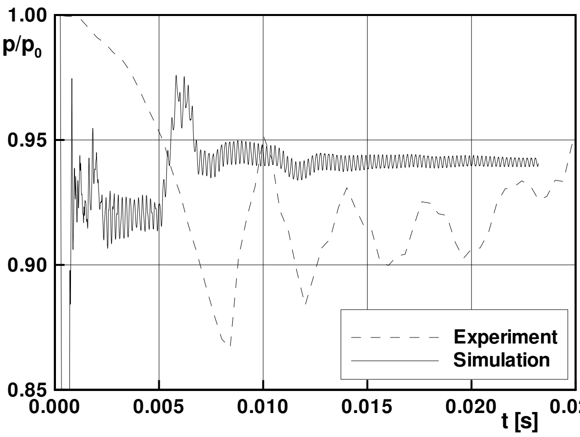

Figure 18. Comparison of pressure variation

Figure 19. Calculated Schlierenpicture at $t = 4.8 \cdot 10^{-5}\,\mathrm{s}$

number of points increases slightly up to 112400 points. The initial conditions are $T_0 = 600\,\mathrm{K}$, $p_0 = 20\,\mathrm{bar}$, $T_{vac} = 295\,\mathrm{K}$ and $p_{vac} = 2\,\mathrm{mbar}$ while again in both regimes the fluid is at rest. Due to restrictions of the solver, the valve cannot be entirely closed on startup. An initial width of 1 mm was chosen with a virtual membrane vanishing in the first timestep. The movement is modelled via grid deformation which was done after each physical time step. The initial and the final boundaries of the computational domain are visible in Fig. 17. When a limit of skewness due to deformation is exceeded, a new grid is created based on the current valve opening. The solution is transferred to the subsequent grid via interpolation. With the cells in the gap between the valve and the nozzle throat being very small the size of the physical timestep is to be reduced to $5 \cdot 10^{-9}\,\mathrm{s}$. In comparison to the simplified geometry the onset of flow is smoother. Additional expansion waves evolve from the moving boundaries and interact with the flow field. The distribution of $|\mathrm{grad}\,\varrho|$ in Fig. 19 shows compression and expansion waves at $t = 4.8 \cdot 10^{-5}\,\mathrm{s}$ after the start of the simulation. While complex structures of shocks and contact discontinuities pass the nozzle throat, expansion waves originating from the annular gap in the piston and the front face of the piston as well as from the initial discontinuity propagate and partially refract at the front of the piston.

The numerical effort for the simulations with valve movement is enormous. While the solver works in parallel mode, mesh deformation and the consecutive preprocessing that generates the dual grids are up to now sequential and slow down the simulation considerably. The tiny cells in the gap between the valve and the nozzle throat impose a very small physical timestep. Thus the time needed for simulating the first $1 \cdot 10^{-4}\,\mathrm{s}$ of a wind tunnel run on 12 cpus (AMD Opteron@2.2 GHz) is approximately 12 days. To allow the simulations to be done in a reasonable amount of time several acceleration means have to be implemented:

- The sequential deformation and preprocessing step takes longer than the parallel run of the solver. Parallelisation of at least the deformation should result in a considerable speedup of the simulation.

- The speed of the valve piston is constant during the simulation and thus the calculated speed of the faces of the control volumes never changes. It will be investigated if the calculation can be skipped and the speed set directly.

- Following an even more aggressive approach, it is investigated if the preprocessing can be skipped for a certain amount of timesteps while the speed of the cell faces is maintained. It will be examined how long the metric of the cells can be frozen without the error increasing too much.

7. CONCLUSIONS

The Hypersonic Ludwieg Tube at Braunschweig is a facility with remarkable low operational cost. Initial temperature measurements in the storage tube revealed a strong stratification accompanied by convectional flow. Both could be minimized by the introduction of an isolating shutter to the end of the heated tube section. The remaining temperature difference over the height of the measurement section is about 20 K which corresponds to a deviation of the Reynolds number by 6.5% at a nominal total temperature of 460 K. The measured distribution of Pitot pressure over the height of the test section deviates by less then $\pm 1.2\%$ from its mean value which is in very good agreement with Navier-Stokes calculations conducted in the course of nozzle design. The nominal Mach number in the center of the test section was calculated to be 5.9.

Preliminary transition tests on a 5° half angle cone revealed only a slight dependence of transition Reynolds number on unit Reynolds number. However, transition onset occured at Reynolds numbers somewhat below the values measured elsewhere which is thought to be due to imperfections of the cone apex. The measurements will be repeated soon. Moreover, measurements of the Pitot pressure fluctuations are planned.

Despite simplifications in the geometry and the modelling of the flow field, instationary numerical simulations tend to show similar pressure oscillations as the measurements do. Employing the actual geometry and especially the piston movement leads to an enourmous numerical effort which up to now inhibits complete simulations. Thus, the examination and implementation of numerical accelerating techniques is under way.

REFERENCES

Albertson C.W., Bausermann Jr. W.A., 1993, Total Temperature Probes for High-Temperature Hypersonic Boundary-Layer Measurements, NASA TM 4407

Becker E., 1966, Gasdynamik, Leifäden der angewandten Mathematik und Mechanik Band 6, Teubner Studienbücher, 1. Aufl., Verl.-Nr. 2035, Stuttgart

Cook W.J., Felderman E.J., 1966, Reduction of Data from Thin-Film Heat-Transfer Gages: A Concise Numerical Technique, AIAA Journal, Vol. 4, No. 3, pp. 561-562

DLR, 2004, Technical Documentation of the DLR TAU-Code, Technical Report

Estorf M., Radespiel R., Heating Rate Calculation from Thermographic Data Considering Lateral Heat Conduction in Plane Surfaces, To be published

Estorf M., Radespiel R., Heine M., Müller-Eigner R., 2003, Der Hyperschallwindkanal Ludwiegrohr Braunschweig HLB, DGLR-Jahrbuch 2003, Vol. 1, pp. 661-670

Koppenwallner G., Müller-Eigner R., Friehmelt H., 1993, HHK Hochschul-Hyperschall-Kanal: Ein "'Low-Cost"' Windkanal für Forschung und Ausbildung, DGLR Jahrbuch, Band II

Kožulović D., Radespiel R., Müller-Eigner R., 2002, Aerodynamic Design Parameters of a Hypersonic Ludwieg Tube Nozzle, Conference Proceedings: West East High Speed Flow Fields, D. E. Zeitoun, J. Periaux, J. A. Désidéri, M. Martin (Eds.)

Ludwieg H., 1955, Der Rohrwindkanal, Z. f. Flugwiss. 3, Nr. 7, pp. 206-216

Mack A., Hannemann V., 2002, Validation of the Unstructured DLR-TAU-Code for Hypersonic Flows, AIAA Paper 2002-3111

Scadron M.D., Gettelmann C.C., Pack G.J., 1950, Performance of Three High-Recovery-Factor Thermocouple Probes for Room-Temperature Operation, NACA RM E50I29

Schneider S.P., 2001, Effects of High-Speed Tunnel Noise on Laminar-Turbulent Transition, Journal of Spacecraft and Rockets, Vol. 38, No. 3, pp. 323-333

Schneider S.P., 2004, Hypersonic laminar-turbulent transition on circular cones and scramjet forebodies, Progress in Aerospace Sciences 40, Elsevier, pp. 1-50